Popular summary

"The "RED versa NIR" plane to retrieve broken-cloud optical depth from ground-based measurements"

A. Marshak (NASA/GSFC), Y. Knyazikhin (Boston University), K. Evans (UMBC), and W. Wiscombe (NASA/GSFC)

(prepared for Journal of the Atmospheric Sciences)

So far all ground-based retrievals of cloud properties assume that clouds vary only vertically, ignoring not only horizontal in-cloud structure but also broken cloudiness. This leads to misinterpretation of cloud properties and often makes their remote sensing impossible. We propose a new technique that retrieves cloud optical thickness for even broken clouds above green vegetation from surface measurements of zenith radiance in the red (RED) and near-IR (NIR) spectral regions. The idea of the method is simple and based on the very different spectral behavior of green vegetation and cloud liquid water drops. Since green vegetation reflects 30-50% of incoming radiation in the NIR and only 5-10% in the RED region, ground measurements under thin clouds have little spectral contrast between RED and NIR, while thick clouds reflect much more of the surface-reflected radiation in the NIR than in RED. Based on this idea, we proposed to use points on the "RED versa NIR" plane for the retrieval of cloud optical thickness.
The proposed retrieval method is applied to Cimel measurements at the Atmospheric Radiation Measurements (ARM) site in Oklahoma. Cimel, a multi-channel sunphotometer, is a part of AERONET - a ground-based network for monitoring aerosol optical properties. When conditions are inappropriate to make AERONET measurements that are suitable for aerosol studies, new measurements related to cloud physics are made instead. As such, several AERONET Cimel sunphotometers have been equipped with a new "cloud mode." This mode allows the Cimels to make measurements of zenith radiance when the Sun in blocked by clouds and thus to monitor cloud properties using the proposed retrieval method.

The "RED versa NIR" plane to retrieve broken-cloud optical depth from ground-based measurements

A. Marshak, Y. Knyazikhin, K. Evans, and W. Wiscombe

(prepared for JAS)

Point-of-contact: A. Marshak (marshak@climate.gsfc.nasa.gov, tel. 301-614-6122).

Abstract

A new method for retrieving cloud optical depth from ground-based measurements of zenith radiance in the RED and near infrared (NIR) spectral regions is introduced. Because zenith radiance does not have a one-to-one relationship with optical depth, it is absolutely impossible to use a monochromatic retrieval. On the other side, algebraic combinations of spectral radiances such as NDCI (Marshak et al., 2000) while largely removing nouniquiness and the radiative effects of cloud inhomogeneity, can result in poor retrievals due to its insensitivity to cloud fraction. Instead, both RED and NIR radiances as points on the "RED vs. NIR" plane are proposed to be used for retrieval. The proposed retrieval method is applied to Cimel measurements at the Atmospheric Radiation Measurements (ARM) site in Oklahoma. Cimel, a multi-channel sunphotometer, is a part of AERONET - a ground-based network for monitoring aerosol optical properties. The results of retrieval are compared with the ones from Microwave Radiometer (MWR) and Multi-Filter Rotating Shadowband Radiometers (MFRSR) located next to Cimel at the ARM site. In addition, the performance of the retrieval method is assessed using a fractal model of cloud inhomogeneity and broken cloudiness. The preliminary results look very promising both theoretically and from measurements.

1. Introduction

The most common approach for retrieving cloud optical depth from ground-based observations uses downwelling fluxes measured by pyranometers in the 0.3- to 3.0- μm region of the solar spectrum (Leontieva and Stamnes, 1994; Boers, 1997). They are relatively cheap and included as standard equipment at many meteorological stations. In addition to broadband pyranometers, there are Multi-Filter Rotating Shadowband Radiometers (MFRSR) that infer the optical properties of clouds using downwelling fluxes measured at one or at several wavelengths in the visible and/or near infrared spectral regions (Min and Harrison, 1996; Leontieva and Stamnes, 1996). The key element in both retrieval techniques is the one-to-one mapping of the "observed" fluxes into cloud optical depth through (the use of) plane-parallel radiative transfer. Both methods are expected to work well only for completely overcast clouds (Ricchiazzi et al., 1995) giving an *effective* optical depth for the whole sky since for inhomogeneous clouds each sky element contributes to the downwelling flux differently (Boers et al., 2000). To infer cloud optical depth locally one can assume to use a narrow-field-of view radiometer

that measures radiances instead of fluxes (Pavloski and Ackerman, 1999). However, lack of one-to-one relationships between radiance and cloud optical depth (e.g., see Fig. 1 in Barker and Marshak, 2001 for zenith radiances), prevents the direct use of radiances measured either.

Recently, Marshak et al. (2000) and Knyazikhin and Marshak (2000) proposed to exploit the sharp spectral contrast in vegetated surface reflectance across 0.7 μm wavelength to retrieve cloud properties from ground-based radiance measurements. The idea is to use ground zenith radiance measurements in two narrow spectral bands on each side of the sharp jump in vegetation albedo near 0.7 μm. Below 0.7 μm in the RED spectral region (648-680) nm), the chlorophyll in green vegetation absorbs 90-95% of solar radiation; thus its albedo is low. On contrast, above 0.7 μm in the near infrared (NIR) spectral region, a green leaf reflects about 90% of incident radiation resulting in a high value of the albedo of vegetated surfaces. In the NIR region, therefore, the green vegetation acts as a powerful reflector illuminating horizontally inhomogeneous clouds from below (see Fig. 5 in Marshak et al. (2000)). This provides the extra information needed to largely remove the ambiguity in measured downwelling radiance caused by radiative effects of the three-dimensional (3D) cloud structure.

The spectral index proposed by Marshak et al. (2000) while substantially eliminates the effect of 3D cloud structure does not carry information on cloud fraction and, in general, can not correctly estimate the total amount of radiation reaching the surface. Thus in addition to zenith radiances, Barker and Marshak (2001) suggested to use downwelling spectral fluxes measured at the surface or from aircraft-based radiometers (Barker et al., 2002). Knowledge of downwelling fluxes substantially improves the retrieval though limits its applicability to sites equipped with MFRSR or other spectral flux measured radiometers (e.g. LI-1800, ASD).

Here we propose a new method for inferring cloud optical depth from spectral zenith measurements without requiring simultaneous measurements of spectral fluxes. Thus it can be used to monitor clouds from remotely located Cimel multi-channel sunphotometers that are the main part in of the AERONET - a ground-based monitoring network that consists of identical multi-channel radiometers for assessing aerosol optical properties and validating their satellite retrievals (Holben et al., 1998).

The idea of the method comes from the "RED versa NIR" method used to retrieve leaf area index (LAI) from satellite measurements (Knyazikhin. et al., 1998; Shabanov et al., 2002). In addition to cloud optical depth, the new retrieval method also infers a "radiatively effective" cloud fraction. Similar approach in remote sensing is a Nakajima-King technique for retrieving cloud optical depth and effective particle radius from (Nakajima and King, 1990).

The plan of the paper is the following. We start from the physical background deduced from Cimel measurements under clear and cloudy conditions (section 2); then we discuss cloud index and its shortcomings (section 3). Section 4 introduces a new method and which will be applied to Cimel data (section 5). Surface reflective properties

as a key element in the retrieval technique is discussed in section 6, while section 7 validates the method using a fractal-based model of cloud inhomogeneity. Finally, section 8 summarizes the results.

2. Three main atmospheric cases observed in ground zenith radiance measurements

For proof-of-concept measurements (Wiscombe et al., 2000), Fig. 1 shows a 22 min fragment of zenith radiance measured by a ground-based Cimel multi-channel sunphotometer pointed straight up. Cimel has a narrow field of view of 1.2° and four filters at 0.44, 0.67, 0.87 and 1.02 μm that are designed for retrieving aerosol properties in clear sky conditions. In our example, Cimel measured radiance at 20 sec. temporal resolution.

There are three distinct regions in Fig. 1: (from left to right) a single unbroken cloud, broken clouds, and a clear sky. For clear sky conditions, due to Rayleigh scattering and optically thicker aerosol at smaller wavelengths, zenith radiance increases with decrease in the wavelength from 1.02 to 0.44 μm. By contrast, for cloudy conditions radiances in channel 0.44 and 0.67 μm are almost indistinguishable; this also true for channels 0.87 and 1.02 μm. This is a clear indication that in the presence of clouds, the spectral contrast in surface albedo dominates over Rayleigh and aerosol effects. In contrast to the small fluctuations typical for clear and even cloudy skies, broken clouds show sharp changes in radiances around cloud edges.

To be more formal, based on photon cloud-vegetation interactions we distinguish three main cases:

(1) *Atmosphere dominates.* In this case,

$$I_{0.44} >> I_{0.67} > I_{0.87} > I_{1.02} \tag{1a}$$

and aerosol optical properties can be retrieved.

(2) *(Vegetated) surface and cloud dominates.* In this case,

$$I_{0.44} \approx I_{0.67} < I_{0.87} \approx I_{1.02} \tag{1b}$$

and cloud optical properties can be retrieved (provided we know the surface albedo).

(3) *Transition between the first two cases*, characterized by rapid changes between the "order" of I_λ from cloudy to clear and back. In this case, neither aerosol nor cloud properties can be reliably retrieved using only *one* wavelength. However, as will be seen below, the two-wavelength retrieval for broken clouds can be almost as successful as for an overcast sky.

3. Cloud Index and its shortcoming

By analogy with Normalized Difference Vegetation Index (NDVI, Tucker, 1979; Verstraete and Pinty, 1996), Marshak et al. (2000) and Knyazikhin and Marshak (2000) proposed to use the Normalized Difference Cloud Index (NDCI) defined as a ratio between the difference and the sum of two normalized zenith radiances measured for two narrow spectral bands in the NIR (0.87 μm) and RED (0.67 μm) spectral regions,

$$NDCI = \frac{I_{NIR} - I_{RED}}{I_{NIR} + I_{RED}}. \quad (2)$$

Compared to a two-valued optical depth versa zenith radiance relationship, that makes its retrieval absolutely impossible (see one-dimensional (1D) curves in Figs. 2a and b), the NDCI is a monotonic function with respect to optical depth (see 1D curves in Fig. 2c). In contrast to any conventional method of estimating cloud optical depth from the surface that uses either broadband (Leontieva and Stamnes, 1994) or a single wavelength (Min and Harrison, 1996; Leontieva and Stamnes, 1996) and is expected to work well only for overcast clouds (Boers et al., 2000), the NDCI-based retrieval technique is much less sensitive to cloud structure. The sensitivity is weak because the NDCI-based method eliminates the part of downward radiation that did not have interactions with surface; this radiation is the most sensitive to both illumination conditions and cloud inhomogeneity (Marshak et al, 2000, Barker and Marshak, 2001). In addition, the NDCI is almost insensitive to the Solar Zenith Angle (SZA); consequently, optical depth of a cloud illuminated under SZA=80^0, can be retrieved as good as the one illuminated under SZA=45^0. This is a valuable feature of a retrieval method since most current techniques fail to perform reliable retrievals for large SZA. The NDCI-based approach first extracts radiation reflected by clouds and then performs retrieval; hence its weak sensitivity to the SZA (compare to Kaufmann et al., 2000 for NDVI).

As follows from Eqs. (1a)-(1b), the NDCI will be negative for a clear sky and positive for an overcast sky. In case of broken clouds, NDCI can take on either positive or negative values, depending whether there is a cloud in the zenith direction or not.

The first shortcoming of the 1D NDCI-based retrieval technique comes from the underestimation of zenith radiance for large optical depth in NIR. Indeed, Figs. 2a and 2b show 3D and 1D zenith radiances calculated for black (RED) and bright surface (NIR). We see that in the RED spectral region, 3D radiances are scattered around a theoretical 1D curve, while in NIR, 1D radiance systematically underestimates 3D radiances for large optical depths. This is understandable since for 3D clouds, more radiation is transmitted through; thus more radiation is reflected back from thick clouds to the surface.

Another shortcoming of the NDCI is the same as for any spectral indices (e.g., Diner et al., 1999; Tian et al., 2000): the spectral information is reduced to one number by algebraic transformation. In other words, instead of *two* spectral values of zenith

radiances in RED and NIR, we keep only *one*, NDCI. Indeed, each point on a RED versa NIR plane has two coordinates:

$$\eta = \sqrt{I_{RED}^2 + I_{NIR}^2} \tag{3a}$$
$$\alpha = \arctan(I_{RED} / I_{NIR}). \tag{3b}$$

However, all points on a RED versa NIR plane with a similar α have the *same*

$$NDCI = \frac{1-\tan\alpha}{1+\tan\alpha} \tag{3c}$$

independent on η. We will show below how this shortcoming can be overcome if both NIR and RED wavelength are used instead of the NDCI.

4. RED versa NIR plane

Any ground measurements of radiance, I, can be represented as a sum of two components (e.g., Box et al., 1988): the radiation calculated for a non-reflecting surface, I_0, and the radiation due to surface-cloud interactions,

$$I = I_0 + \frac{\rho T_0 I_s}{1-\rho R}. \tag{4}$$

Here, R is the spherical albedo for isotropically illuminated clouds, T_0 is the transmittance for non-reflecting surface, and I_s is the radiance generated by an isotropic source located at the surface with albedo ρ.

Following Baker and Marshak (2001) we will define T_0 and R as

$$T_0 = T_{\text{clear}}(1\text{-}A_c) + T_{\text{cloudy}}A_c, \tag{5a}$$
$$R = R_{\text{clear}}(1\text{-}A_c) + R_{\text{cloudy}}A_c, \tag{5b}$$

where A_c is a cloud fraction. Assuming for simplicity that $T_{\text{clear}} = 1$, $T_{\text{cloudy}} = T_{0pp}$, $R_{\text{clear}} = 0$, and $R_{\text{cloudy}} = R_{pp}$, where T_{0pp} and R_{pp} are plane-parallel transmittance for non-reflecting surface and isotropic albedo, respectively. Thus, Eqs. (5a) –(5b) can be rewritten as

$$T_0 = 1\text{-}A_c + T_{0pp}A_c, \tag{6a}$$
$$R = R_{pp}A_c. \tag{6b}$$

Now we assume that in Eq. (4) only surface albedo ρ is wavelength dependent while I_0, I_s, T_0 and R are functions of only cloud optical depth τ. It follows from these assumptions and from (6a) –(6b) that

$$I_{RED}(\tau, A_c) = I_0(\tau) + \frac{\rho_{RED} I_s(\tau)[1 - A_c + A_c T_{0pp}(\tau)]}{1 - \rho_{RED} A_c R_{pp}(\tau)} \tag{7a}$$

and

$$I_{NIR}(\tau, A_c) = I_0(\tau) + \frac{\rho_{NIR} I_s(\tau)[1 - A_c + A_c T_{0pp}(\tau)]}{1 - \rho_{NIR} A_c R_{pp}(\tau)}. \tag{7b}$$

Let us consider Eq. (6a). It is easy to show that

$$0 \le T_{0pp} \le T_0 \le 1 \tag{8}$$

if

$$0 \le A_c \le 1. \tag{9}$$

The middle inequality in (8) expresses a common knowledge that transmittance for inhomogeneous (or broken) clouds is larger than its plane-parallel counterpart. However, it is also known that for broken clouds transmittance can exceed unity because of photons scattered downwards from cloud edges. Thus the last inequality in (8) is not necessarily hold for broken clouds. To illustrate this, Fig. 3 shows broadband measurements of downward flux for two days in August 1997. We can clearly see that downward flux for broken clouds (between 9 and 10 a.m. on Aug. 17 and around noon on Aug. 15) exceeds the one for clear sky thus producing transmittance larger than 1. More accurately, at 12:05 and SZA=19.2 on Aug. 15 the transmittance even exceeds 1.2. Can this effect be simulated in the frame of plane-parallel radiative transfer?

Indeed, if one releases condition (9) and allows "cloud fraction" to be negative then, as it follows from Eq. (6a), T_0 will exceed 1 and be able to simulate reflectance from cloud edges. Not surprisingly that in this case, T_0 as a function of optical depth looks more like reflectance than transmittance (convex vs. concave). Figure 4 shows T_0 as a function of τ and A_c. Note that $A_c = 0$ gives $T_0 = 1$ while negative A_c correspond to $T_0 > 1$.

To illustrate this behavior Fig. 5a shows an 8-km fragment of a simulated broken cloud field. As expected, the cloud edge around 38.4 km looks much brighter than the rest of the cloud for both RED and NIR radiation. However, when one moves away from the cloud edge, I_{RED} decays much faster than I_{NIR}. Only about 300 m away from the edge, I_{RED} has been already stabilized while I_{NIR} is still strongly affected by the illumination by the bright surface. (Note from the 1D curves in Figs. 2a and 2b that $\max(I_{RED}) = 0.53$ while $\max(I_{RED}) = 0.62$). No positive A_c is able to model this effect in the frame of plane-parallel theory. Indeed, panel 5b shows a 2D Look-Up-Table (LUT) of I_{NIR} versa I_{RED} as functions of τ and A_c described by Eqs. (7a) - (7b). We see that the data-points that are above the $A_c = 0$ curve need negative A_c to be matched by 1D calculations! Obviously, these data-points correspond to transmittance $T_0 > 1$. Also note that all cloudy data-points as well as the LUT itself is above the diagonal $I_{NIR} = I_{RED}$, i.e. $I_{NIR} > I_{RED}$. The same data-points and LUT will occupy the whole plane if the difference $I_{NIR} - I_{RED}$ is plotted against I_{RED} or the sum $I_{NIR} + I_{RED}$. The later one (panel 5c) is preferable since any line through the origin point (0,0) corresponds to NDCI defined in Eq. (2).

As an example, Fig. 6a shows a NIR-RED versa NIR+RED plane with real Cimel measurements at the Atmospheric Radiation Measurements (ARM) site in Oklahoma (97.48° W, 36.61° N) on July 28, 2002. For SZA = 62^0 and surface albedos ρ_{RED}=0.092 and ρ_{NIR}=0.289, it illustrates a DISORT calculated LUT with I_{NIR} and I_{RED} as functions of τ and A_c, and three groups of data-points (10 points per a group, see next section for explanations) measured by Cimel. The data-points, while having different values of I_{NIR} and I_{RED} thus being located at different positions on the plane, have almost the same NDCI (a straight line through the point (0,0)); hence the same optical depth τ (80 for A_c= 1.0). However, as it follows from the LUT, these groups correspond to different pairs: (A_c=0.9; τ=28), (A_c=0.8; τ=22), and (A_c=0.4; τ=12); thus have different optical depths. Figure 6b shows a Total Sky Image (TSI) taken at 14:00 UMT close to the middle cluster of points in panel 6a. Note that A_c= 0.8 is not a "real" cloud fraction but rather a "radiatively effective" one in the sense that 1D radiative transfer gives the same values of I_{NIR} and I_{RED} as the measured (3D) ones.

The LUTs shown in Fig. 6 and Figs. 5b and 5c for retrieval cloud optical depth and cloud fraction can be viewed as a ground-based counterpart of the Nakajima-King retrieval of cloud optical depth and effective particle radius from reflected solar radiation (Nakajima and King, 1990). In the Nakajima-King retrieval, visible channel is more sensitive to cloud optical depth and less sensitive to a particle size while the absorbing NIR channel is more sensitive to a particle size than to optical depth. Similar, for the ground-based retrieval above vegetation, the RED channel is much more sensitive to optical depth while the NIR is more sensitive to cloud fraction. Next section will discuss the retrievals in more details.

5. Retrieval from Cimel measurements

Cimel spectrometers are the main instruments in the AERONET - a ground based monitoring network that consists of identical multi-channel radiometers for assessing aerosol optical properties and validating their satellite retrievals (Holben et al., 1998). Based on the above ideas, we have developed a method for Cimels to monitor cloud optical depth by using "idle time" inappropriate for aerosol studies for taking measurements of zenith radiance at 0.44, 0.67, 0.87 and 1.02 μm. Every 13 min, if the Sun is blocked by clouds, the Cimel points straight up and takes 10 measurements with a 9 sec. time interval.

The main idea of our method is to retrieve cloud optical depth using both 0.67 μm (RED) and 0.87 μm (NIR) zenith radiances; surface albedos ρ_{RED} and ρ_{NIR} are assumed to be known from independent measurements. Other two channels (0.44 and 1.02 μm) are used to select cases where the spectral contrast in surface albedo dominates over Rayleigh and aerosol effects (i.e., when Eq. (1b) is hold) and the proposed method will likely work. Another consistency check is related to Cimel's second collimator that has the same field of view of 1.2^0 but 10 times larger aperture; thus it sees different cloud pieces.

Figure 7a illustrates the retrieval of cloud optical depth from Cimel measurements using the above method. The retrieved optical depths are also compared with the ones from MicroWave Radiometer (MWR) (assuming a constant droplet effective radius of 10 μm) and from Multi-Filter Rotating Shadowband Radiometer (MFRSR) (courtesy of Q. L. Min; for details see Min and Harrison, 1996). For this overcast day, generally we see very good agreement, though there are a few discrepancies. For the most homogeneous plane-parallel cloud around 14:30 UMT (panel 7b1) all three methods show similar optical depth τ around 20; the LUT in Fig. 7b2 estimates the radiatively effective cloud fraction A_c as 0.8. For more inhomogeneous though still overcast clouds as the one at 17:50 (panel 7c1) the agreement is not as good as for the homogeneous cloud since MFRSR retrieves a more effective optical depth (in its field of view) than our algorithm does. Figure 7c2 shows the LUT with scattered Cimel dots; the most inhomogeneous part (at 17:52) corresponds to the largest difference between I_{NIR} and I_{RED} that estimates $A_c \approx 0.5$ and $\tau \approx 90$.

Another example (Fig. 8a) corresponds to broken clouds (Figs. 8b and 8c). There are two remarkable features highlighted in this day. First, the optical depth is retrieved for SZA=81^0 (at 12:30-12:40, see panel (b)); this is not very common for any (satellite or ground-based) optical depth retrievals. Second, it is retrieved for very broken-cloud conditions; the cloud optical depth for 30 min. jumps from almost 0 (17:52) to 90 (18:08) and then backs to clear sky (18:22). This is also shown in Fig. 8d where we see the rapidly changing order of Cimel zenith radiances as in Fig. 1 and Eqs. (1a) - (1b). As expected, the optical depth field retrieved from MFRSR around 18:00 is much smoother and represents an "effective" optical depth for the sky shown in panel (c).

6. Surface

Since the retrieval algorithm is based on surface-cloud interaction, knowledge of surface reflectance and its heterogeneity around Cimel is absolutely crucial for the success of the algorithm.

To estimate surface albedo we use Moderate Resolution Imaging Spectroradiometer (MODIS) data averaged over 16 days (Schaaf et al., 2002). Figure 9 illustrates surface albedo for 0.648 and 0.858 μm around the ARM site for July 28, 2002. The average values are about 0.09 for 0.648 μm and 0.29 for 0.858 μm; they are consistent with Multi-angle Imaging Spectro-Radiometer (MISR) data (REFERENCE) retrieved on July 24, 2002 ($\rho_{0.672} = 0.12$, $\rho_{0.867} = 0.28$; averaged over $(27.5\ km)^2$: $\langle\rho_{0.672}\rangle = 0.10$ with standard deviation (sdev) = 0.02 and $\langle\rho_{0.867}\rangle = 0.28$ with sdev=0.03. Pavloski et al. (2002) used MISR surface albedo data to retrieve cloud optical depth from simultaneous measurements of downward radiance and flux at the ARM site in Oklahoma applying algorithm proposed by Barker and Marshak (2001).

For the theoretical study based on cloud fields inferred from Landsat imagery, Baker and Marshak, (2001) found that as long as the uncertainties in surface albedo have the same sign (both are either overestimated or underestimated), the algorithm performs

well. Furthermore, when the NIR albedo is overestimated but the RED albedo is underestimated, errors in the retrieved optical depth are not severe. However, in the opposite case, the algorithm underestimates multiple reflectance in the bright band and greatly overestimates optical depths. A detailed analysis of the sensitivity to surface albedo can be found in Beaulne et al. (2003). Similar tendencies are also valid for the present algorithm.

Surface reflectance at the ARM site in Oklahoma is very heterogeneous (Li et al., 2002). Figure 10 is based on Solar Spectral Flux Radiometer (SSFR) data (Pilewskie et al., 2003) reported in Michalsky et al. (2003). It shows surface albedo in RED and NIR spectral regions measured on flight legs covering the area of about 25 km around the ARM site (panel (a)) on April 5, 2000. In addition, data for the nearest 0.0001 radian (about 600 m) to the site was also selected. We see that the range of surface albedos in the area of 1 km around Cimel on that day was from 0.056 to 0.118 for the RED and from 0.325 to 0.434 for the NIR with $\rho_{RED} = 0.085 \pm 0.013$ and $\rho_{NIR} = 0.375 \pm 0.021$. These average results are not necessarily match surface albedo measured from 10-m and 25-m towers located exactly at the ARM site over wheat and (dead) grass (Li et al., 2002, Michalsky et al., 2003). However, the big range in surface albedos does not prevent the use of the proposed method since the contribution from surface is integrated over several km (depending on cloud base height) and the local surface properties are less important than its average or "effective" characteristics (Knyazikhin and Marshak, 2000). It can be shown that in spite of strong surface heterogeneity the value of surface reflectivity around the ARM site stabilizes after averaging over 1 – 2 km for both RED and NIR spectral regions (Wiscombe et al., 2000).

7. Validation

In addition to validation with retrievals from other ground-based measurements (MWR and MFRSR) that are illustrated in Figs. 7 and 8, we show a model-based validation where the true value of optical depth is known. We used 10 realizations of a 10-cascade fractal cloud model of broken clouds from Cahalan et al., 1994 and Marshak et al., 1998 (see Fig. 2 captions for details). The cloud fraction was 81% and the total number of nonzero cloud optical thicknesses was ($0.81 \times 2^{10} \times 10 \approx 8300$). The average in-cloud τ was 13 with standard deviation of 10.5. For simplicity, we had "black" and "bright" surface with albedos $\rho_{RED} = 0.0$ and $\rho_{NIR} = 0.5$, respectively. The domain averaged retrieved values for oblique illumination of SZA = 60° and conservative scattering gave very close results of mean 13.1 and standard deviation 10.8.

Figure 11a shows a scatter plot of retrieved versa true optical depth on a pixel-by-pixel basis for a pixel size of 25 m. We see that while the "NDCI" method overestimates cloud optical depth values especially for $\tau > 20$ and shows a lot of saturated values of $\tau = 100$, the "RED vs. NIR" method gives on average unbiased estimates. When averaged over 8 pixels (200-m resolution pixels), the retrieval substantially improves (Fig. 11b); the average absolute error in τ is 1.8 down from 2.4 (3.0 for in-cloud pixels) for 25-m resolution pixels.

Finally, Figs. 12a and b illustrate histograms of cloud optical depth (true and retrieved) on a lin-lin and log-line scale, respectively. We can clearly see that the "RED vs. NIR" method correctly retrieves the distribution of τ for both small and large values. Analyzing the cumulative histogram of absolute errors (Fig. 13) we can conclude that in 50% cases the absolute error in the retrieval of optical depth is smaller than 1, in 75% cases smaller than 3, and in 90% cases is smaller than 5. In contrast, the "NDCI" method strongly overestimates the retrieved values for at least $\tau > 40$; this makes it completely unacceptable for the retrieval of large τ.

8. Summary

Ground-based remote sensing of cloud optical properties with broadband pyranometers (e.g., Leontieva and Stamnes, 1994) and/or narrowband radiometers (Min and Harrison, 1996) that measure downwelling fluxes is limited to overcast conditions (Boers et al., 2000). Retrieved values of cloud optical depth have an effective rather a local character (Barker and Marshak, 2001). Monochromatic narrow field-of-view measurements are not widely applicable for retrieval because cloud optical depth is a two-value function of zenith radiance. Among others these shortcomings prevent us from creating a ground-based cloud properties monitoring network as the AERONET for assessing aerosol properties (Holben et al., 1998).

To remove the ambiguity in measured downwelling radiance, it was suggested to exploit a spectral contrast in surface properties between RED and NIR spectral regions (Marshak et al., 2000). An algebraic combination of NIR and RED zenith measurements or, the so-called Normalized Difference Cloud Index (NDCI), largely removes not only the double valued relationship between radiance and optical depth but also the radiative effects of the 3D cloud structure. However for accurate retrievals it requires additional information on downwelling fluxes (Barker and Marshak, 2001 and Barker et al., 2002) and the NDCI (or other similar indices) along cannot be used for broken cloud conditions.

Here we proposed a new method that overcomes the limitations of the NDCI; instead of using one value of an algebraic combination between two wavelengths, we use both wavelengths independently in the NIR vs. RED plane. Mapping NIR and RED measurements of zenith radiance into a two-dimensional plane-parallel radiative transfer based look-up-table (LUT) allowed us not only to retrieve cloud optical depth τ but also to estimate cloud fraction A_c. However, since plane-parallel radiative transfer is unable to fit all 3D measurements (for example, leakage from cloud edges results in cloud transmittance larger than unity), instead of a "real" cloud fraction (the ratio of cloudy pixels to the total number of pixels) we retrieve a radiatively *effective* cloud fraction (or index of local cloud inhomogeneity) that matches 3D measurements with 1D calculations. This does not preclude it from to be *negative*. The retrieved values A_c are not used *per se* but as a degree of cloud inhomogeneity for the retrieval of cloud optical depth.

This method assumes that surface albedo in both RED and NIR spectral regions is known. Because of the proposed *global* character of the cloud monitoring network, the high resolution satellite data is the only available source of surface properties. As an example, here we applied MODIS surface albedo data averaged over 16 days. Even in case of heterogeneous surface as the one around the ARM site in Oklahoma (Li et al., 2002; Michalsky et al., 2002), we found that the proposed method can be successfully used since the local surface properties are less important than their average characteristics (Knyazikhin and Marshak, 2000).

In addition to the comparison with MFRSR (courtesy of Qilong Min) and MWR retrievals (the later needs an assumption on the drop size) that are located next to Cimel at the ARM site, we used realizations of a fractal model of cloud inhomogeneity (Cahalan et al., 1994) and of broken clouds (Marshak et al., 1998). Since the "true' optical depth was known, we were able to validate the performance of the proposed method. 75 % of the retrieved optical depth out of about 10000 pixels with 25 m resolution had absolute errors smaller than 3. Averaging over 200 m substantially improves the retrieval.

To conclude, the preliminary results look very promising both theoretically and from measurements. As soon as the method matures, it will be systematically applied to AERONET "cloud" measurements that are inappropriate for aerosol studies to monitor cloud optical depth.

Acknowledgments. This work was supported by the Department of Energy (under grant DE-A105-90ER61069 to NASA's GSFC) as part of the Atmospheric Radiation Measurement (ARM) program, and by NASA's Radiation Program Office (under grant NAG5-11373). We thank H. Barker, E. Clothiaux, A. Davis, C. Pavloski, and T. Varnai for stimulating discussions, M. Miller, B. Holben, I. Slutsker for help with Cimel data, Q. Min for MFRSR retrieval, and A. Trishchenko for Fig. 10a.

Figure Captions

Figure 1. Zenith radiance measured by a Cimel sunphotometer at Greenbelt, MD on May 24, 1999. Four channels 0.44, 0.67, 0.87 and 1.02 μm are used. The measured radiance is normalized by the solar flux at the TOA in the corresponding spectral interval.

Figure 2. Downward radiances calculated by Monte Carlo methods for "black" surface (RED, $\rho = 0.0$, panel (a)), and "bright" surface (NIR, $\rho = 0.5$, panel (b)). Pixel size is 25 m, SZA = 60°, $\varpi_0 = 1.0$, Henyey-Greenstein scattering phase function. Horizontal distribution of cloud optical depth is simulated by a 10-steps bounded cascade model (Cahalan et al., 1994) with parameters $\langle\tau\rangle = 13$, $\beta = 1.4$ and $p = 0.35$. The average geometrical cloud thickness is 300 m; cloud base height is 1 km. Holes are added as in Marshak et al. (1998). The results of 1D radiative transfer calculations from DISORT (Stamnes et al., 1988) are added for convenience. (c) The same as in panels (a) and (b) but for the NDCI defined by Eq. (2).

Figure 3. Ground based measurements of downward radiation at La Jolla, CA in August, 1997. Left panel is typical for La Jolla: early morning overcast sky, then broken cloudiness that clears up by noon. Right panel represents an almost entirely overcast day with a few scattered clouds around noon. Solar zenith angles are added for clarity.

Figure 4. Transmittance T_0 as a function of optical depth τ and cloud fraction A_c. Horizontal axis consists of 15 ranges of τ from 0 to 100. Each τ-range corresponds to different A_c from $A_c = 1$ to $A_c = -0.4$ including the case of $A_c = 0$ which corresponds to $T_0 = 1$.

Figure 5. Zenith radiances I_{RED} and I_{NIR} for the same model as in Fig. 2. (a) An 8-km fragment of I_{RED}, I_{NIR} (top panel, right vertical axis), and optical depth τ (bottom panel, left vertical axis) versa horizontal position x (km). (b) Zenith radiances for RED and NIR as functions of optical depth τ and cloud fraction A_c [Eqs. (7a) and (7b)] calculated using DISORT (Stamnes et al., 1988); τ changes from 0.5 to 100 while A_c changes from 0.0 to 1.0. Note that both I_{RED} and I_{NIR} are double-value functions with respect to τ. Dots correspond to data-points from panel (a) between 38.8 ($I_{NIR} < 0.8$) and 44 km (208 dots). (c) The same as in panel (b) but for NIR-RED versa NIR+RED.

Figure 6. NIR-RED versa NIR+RED plane with Cimel radiances measured at the ARM Oklahoma site on July 28, 2002. (a) SZA = $62^0 \pm 3^0$ and surface albedos ρ_{RED}=0.092 and ρ_{NIR}=0.289. I_{RED} and I_{NIR} are calculated using DISORT. Optical depth τ changes from 0.5 to 80 while cloud fraction A_c changes from 0.2 to 1.0. 30 dots (10 for each cluster) correspond to Cimel measurements taken around 13:45, 13:58, and 14:11 UMT, respectively (towards decreasing NIR+RED). A straight line through (0,0) is the NDCI ≈ 0.08. (b) a Total Sky Image taken at 14:00 UMT with SZA=62.75^0.

Figure 7. Retrievals for July 3, 2002 at the ARM Oklahoma site. (a) retrievals based on MWR (assuming droplet effective radius of 10 μm), Cimel radiances (using reflectances from a vegetated surface with albedos ρ_{RED}=0.119 and ρ_{NIR}=0.302), and MFRSR fluxes (using algorithm proposed in Min and Harrison, 1996). (b1) a Total Sky Image for SZA = 52.3^0 taken at 14:36 UMT. (b2) LUT for SZA = 53^0 ± 1^0. Optical depth τ changes from 0.5 to 100 with increment of 2.5 while cloud fraction A_c changes from -0.6 to 1.0 with increment of 0.2. 20 dots correspond to Cimel measurements taken between 14:30-14:37 UMT. (c1) the same as in (b1) but for SZA = 16.3^0 taken at 14:50 UMT. (c2) the same as in (b2) but for SZA = 16^0 ± 1^0. 20 Cimel measurements were taken between 17:43-17:52 UMT.

Figure 8. Retrievals for August 8, 2002 at the ARM Oklahoma site. (a) retrievals based on MWR (assuming droplet effective radius of 10 μm) and Cimel radiances (surface albedos are ρ_{RED}=0.096 and ρ_{NIR}=0.338). (b) a Total Sky Image for SZA = 79.6^0 taken at 12:40 UMT. (c) the same as in (b) but for SZA = 21.9^0 taken at 18:00 UMT. (d) 30 min. of normalized Cimel zenith radiances at four channels: 0.44, 0.67, 0.87 and 1.02 μm.

Figure 9. Surface albedo retrieved from MODIS on July 28, 2002. 25 by 25 km^2 area around the ARM site in Oklahoma; its location is at (0,0). (a) 0.648 μm, at the ARM site $\rho_{0.648}$ = 0.092, averaged over (25 km)^2 $\langle\rho_{0.648}\rangle$ = 0.091 with standard deviation (sdev) = 0.016. (b) 0.848 μm; at the ARM site $\rho_{0.858}$ = 0.289, averaged over (25 km)^2 $\langle\rho_{0.858}\rangle$ = 0.292 with sdev = 0.043.

Figure 10. Surface around the ARM site in Oklahoma. (a) Area around the ARM site with a daisy pattern flown by the Twin Otter aircraft on April 5, 2000 (courtesy of Alexander Trishchenko). (b) Surface albedo at 0.86 μm versa 0.66 μm measured from the aircraft by SSFR on April 5, 2000 (for details see Michalsky et al., 2003). Small gray dots correspond to all data collected around the area shown in panel (a) (roughly 10-15 km from the ARM site). Big black dots are the closest to the ARM site measurements (several middle points) taken within 0.0001 radian from the site (around 600 m). For them, $\langle\rho_{0.66}\rangle$ = 0.085, sdev = 0.013 and $\langle\rho_{0.86}\rangle$ = 0.375, sdev = 0.021.

Figure 11. Scatter plot of retrieved versa true cloud optical depth for the same bounded cascade model as in Fig. 2 (Cahalan et al., 1994, Marshak et al., 1998). Cloud fraction is 81%. Ten realizations of bounded cascades are used. SZA = 60°, Two retrieval methods are compared: the "NDCI" and the "RED vs. NIR". (a) original resolution of 25 m. (b) averaged over 200 m.

Figure 12. Histogram of cloud optical depth τ from Fig. 11a. Pixel resolution is 25 m. (a) lin-lin plot. (b) log-lin plot.

Figure 13. Cumulative histogram of absolute errors in the retrieval of cloud optical depth from Fig. 11a. Pixel resolution is 25 m.

References

Barker, H. W., and A. Marshak, 2001: Inferring optical depth of broken clouds above green vegetation using surface solar radiometric measurements. *J. Atmos. Sci.*, **58**, 2989-3006.

Barker, H., A. Marshak, W. Szyrmer, A. Trishchenko, J.-P. Blanchet, and Z. Li, 2002: Inference of cloud optical properties from aircraft-based solar radiometric measurements. *J. Atmos. Sci.*, **59**, 2093-2111.

Beaulne, A., H. W. Barker, J.-P. Blanchet, 2003: Estimating cloud optical depth from surface radiometric observations: sensitivity to droplet phase function, surface albedo, instrument noise, and aerosol. Submitted to *J. Geophys. Res.*

Boers, R., 1997: Simultaneous retrievals of cloud optical depth anddroplet concentration from solar irradiance and microwave liquid. *J. Geophys. Res.*, **102**, 29 881–29 891.

Boers, R., A. van Lammeren, and A. Feijt, 2000: Accuracy of optical depth retrieval from ground-based pyranometers, *J. Atmos. and Ocean. Tech.*, **17**, 916-927.

Box, M. A., S. A. W. Gerstl, and C. Simmer, 1988: Application of the adjoint formulation of the calculation of atmospheric radiative effects. *Beitr. Phys. Atmosph.*, **61**, 303–311.

Cahalan, R. F., 1994: Bounded cascade clouds: Albedo and effective thickness. *Nonlinear Processes in Geoph.*, **1**, 156–167.

Diner, D.J., Asner, G.P., Davies, R., Knyazikhin, Y., Muller, J.P., Nolin, A. W., Pinty, B., Schaaf, C.B., and Stroeve, J., 1999: New directions in Earth observing: Scientific application of multi-angle remote sensing. *Bull. Amer. Meteorol. Soc.*, **80**, 2209-2228

Holben B. N., Eck T. F., Slutsker I., Tanre D., Buis J. P., Setzer A., Vermote E., Reagan J. A., Kaufman Y. J., Nakajima T., Lavenu F., Jankowiak I., Smirnov A., 1998: AERONET - A federated instrument network and data archive for aerosol characterization. *Remote Sens. Environ.*, **66**, 1–16.

Kaufmann, R. K., L. Zhou, Y. Knyazikhin, N. Shabanov, R. B. Myneni, and C. J. Tucker, 2000: Effect of Orbital Drift and Sensor Changes on the Time Series of AVHRR Vegetation Index Data. *IEEE Trans. Geosc. and Remote Sens.*, **38**, 2584-2597.

Knyazikhin, Yu., and A. Marshak, 2000: Mathematical aspects of BRDF modeling: Adjoint problem and Green's function. *Remote Sens. Review*, **18**, 263-280.

Knyazikhin, Y., J. V. Martonchik, D. J. Diner, R. B. Myneni, M. M. Verstraete, B. Pinty, and N. Gobron, 1998: Estimation of vegetation canopy leaf area index and fraction of absorbed photosynthetically active radiation from atmosphere-corrected MISR data. *J. Geophys. Res.*, **103**, 32239-32256.

Leontieva, E., and K. Stamnes, 1994: Estimations of cloud optical thickness from ground-based measurements of incoming solar radiation in the Arctic. *J. Climate*, **7**, 566–578.

Leontieva, E., and K. Stamnes, 1996: Remote sensing of cloud optical properties from ground-based measurements of transmittance: a feasibility case. *J. Appl. Meteor.*, **35**, 2012–2022.

Li, Z.-Q., M.C. Cribb, and A.P. Trishchenko, 2002: Impact of surface inhomogeneity on solar radiative transfer under overcast conditions. *J. Geophys. Res.*, **107 (D16)**, art. no. 4294.

Marshak, A., A. Davis, W. J. Wiscombe, W. Ridgway, and R. F. Cahalan, 1998: Biases in shortwave column absorption in the presence of fractal clouds. *J. Climate*, **11**, 431–446.

Marshak, A., Knyazikhin, Yu., Davis, A., Wiscombe, W., and Pilewskie, P., 2000: Cloud – vegetation interaction: Use of normalized difference cloud index for estimation of cloud optical thickness. *Geoph. Res. Lett.*, **27**,1695-1698.

Michalsky J., Q. Min, J. Barnard, R. Marchand, and P. Pilewskie, 2003: Simultaneous spectral albedo measurements near the Atmospheric Radiation Measurement Southern Great Plains (ARM SGP) central facility. *J. Geophys. Res.*, **108**, 4254, doi:10.1029/2002JD002906.

Min, Q. L., and L. C. Harrison, 1996: Cloud properties derived from surface MFRSR measurements and comparison with GOES results at the ARM SGP site. *Geophys. Res. Lett.*, **23**, 1641–1644.

Nakajima, T. Y., and M. D. King, 1990: Determination of the optical thickness and effective particle radius

of clouds from reflected solar radiation measurements – Part I, Theory. *J. Atmos. Sci.*, **47**, 1878–1893.

Pavloski, C. F., Clothiaux, E. E., Barker, H. W., Marshak, A., Ackerman, T. P., 2002: Field test of the cloud-surface interaction based broken cloud field optical depth retrieval: results from the ARM SGP 2001 Summer-Fall NFOV campaign. (ARM) Science Team Meeting, April 8-12, 2002, St. Petersburg (FL).

Pavloski, C. F. and T. P. Ackerman, 1999: High speed cloud optical depth retrievals from a narrow field of view, narrowband, shortwave zenith pointing radiometer. (ARM) Science Team Meeting, March 22-26, 1999, San Antonio (TX) (available at http://www.arm.gov/docs/documents/technical/conf_9903/pavloski-99.pdf).

Ricchiazzi, P., C. Gautier, D., Lubin, 1995: Cloud scattering optical depth and local surface albedo in the Antarctic - simultaneous retrieval Using ground-based radiometry. *J. Geophys. Res.*, **100**, 21091-21104.

Schaaf C. B., F. Gao, A.H. Strahler, W. Lucht, X.W. Li, T. Tsang, N.C. Strugnell, X.Y. Zhang, Y.F. Jin, J.P. Muller, P. Lewis, M. Barnsley, P. Hobson, M. Disney, G. Roberts, M. Dunderdale, C. Doll, R.P. d'Entremont, B.X. Hu, S.L. Liang, J.L Privette, and D. Roy, 2002: First operational BRDF, albedo nadir reflectance products from MODIS. *Remote Sens. Environ.*, **83**, 135-148.

Shabanov, N.V., L. Zhou, Y. Knyazikhin, C.J. Tucker , R.B. Myneni, R.B., 2002: Analysis of interannual changes in northern vegetation activity observed in AVHRR data during 1981 to 1994. *IEEE Trans. Geosci. Remote Sens.* **40**, 115-130.

Stamnes, K., S.–C. Tsay, W. J. Wiscombe and K. Jayaweera, 1988: Numerically stable algorithm for discrete-ordinate-method radiative transfer in multiple scattering and emitting layered media. *Appl. Opt.*, **27**, 2502–2512.

Tian, Y., Zhang, Y., Knyazikhin, Y., Myneni, R.B., Glassy, J., Dedieu, G., and Running, S.W., 2000: Prototyping of MODIS LAI and FPAR algorithm with LASUR and LANDSAT data. *IEEE Trans. Geosci. Remote Sens.*, **38**, 2387-2401.

Tucker, C. J., 1979: Red and photographic infrared linear combination for monitoring vegetation. *Remote Sens. Environ.*, **8**, 127–150.

Verstraete, M. M., and B. Pinty, 1996: Designing optical spectral indexes for remote sensing applications. *IEEE Trans. Geoscience Rem. Sensing*, **34**, 1254-1265.

Wiscombe, W., A. Marshak, Y. Knyazikhin, and A. Davis, 2000. The Use of Reflection from Vegetation for Estimating. Broken-Cloud Optical Depth. In *Proceedings of the 10th Atmospheric Radiation Measurement (ARM) Science Team Meeting*, March 13-17, 2000, San Antonio (TX), (available at http://www.arm.gov/docs/documents/technical/conf_0003/wiscombe-wj.pdf).

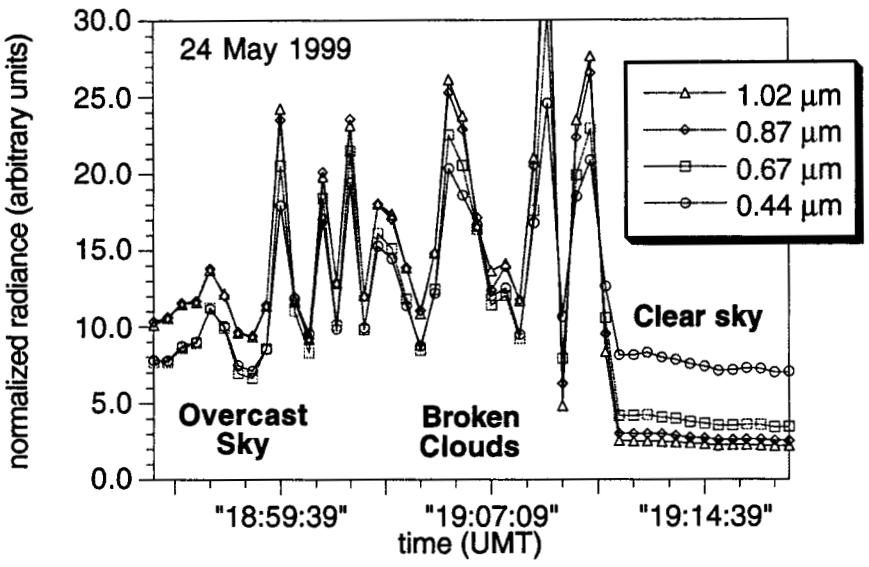

Figure 1. Zenith radiance measured by a Cimel sunphotometer at Greenbelt, MD on May 24, 1999. Four channels 0.44, 0.67, 0.87 and 1.02 μm are used. The measured radiance is normalized by the solar flux at the TOA in the corresponding spectral interval.

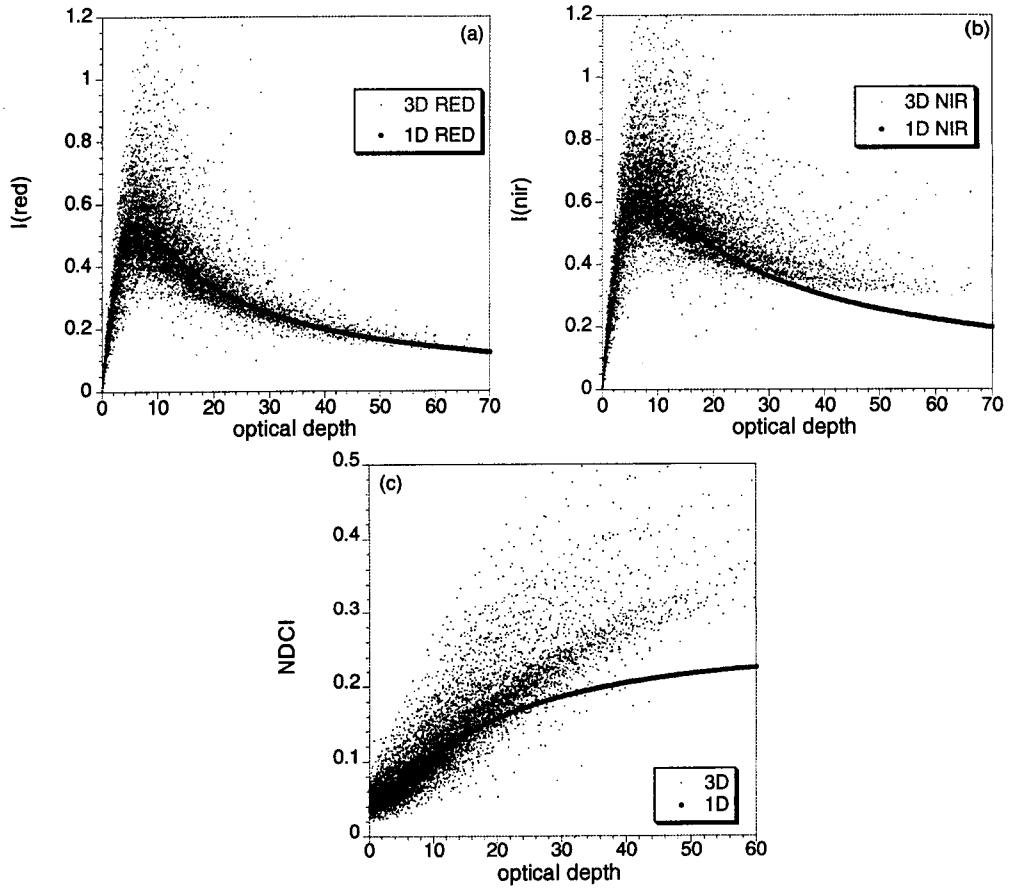

Figure 2. Downward radiances calculated by Monte Carlo methods for "black" surface (RED, $\rho = 0.0$, panel (a)), and "bright" surface (NIR, $\rho = 0.5$, panel (b)). Pixel size is 25 m, SZA = 60°, $\varpi_0 = 1.0$, Henyey-Greenstein scattering phase function. Horizontal distribution of cloud optical depth is simulated by a 10-steps bounded cascade model (Cahalan et al., 1994) with parameters $\langle\tau\rangle = 13$, $\beta = 1.4$ and $p = 0.35$. The average geometrical cloud thickness is 300 m; cloud base height is 1 km. Gaps are added as in Marshak et al. (1998). The results of 1D radiative transfer calculations from DISORT (Stamnes et al., 1988) are added for convenience. (c) The same as in panels (a) and (b) but for the NDCI defined by Eq. (2).

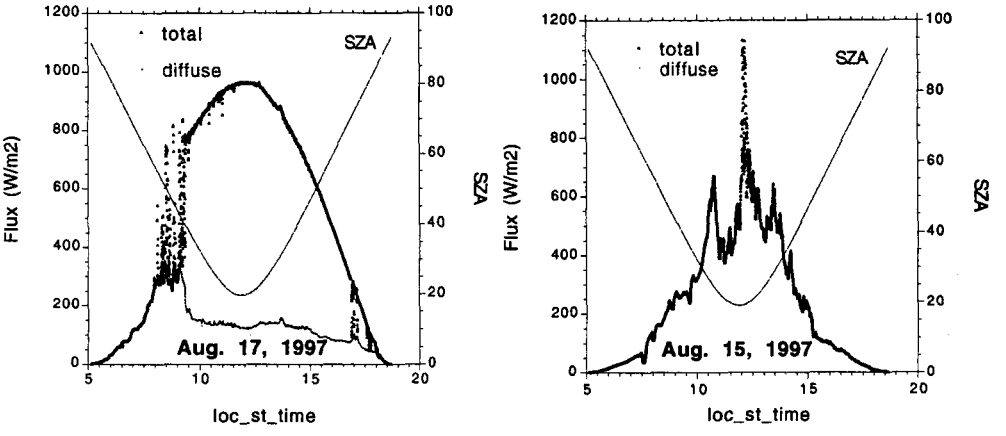

Figure 3. Ground based measurements of downward radiation at La Jolla, CA in August, 1997. Left panel is typical for La Jolla: early morning overcast sky, then broken cloudiness that clears up by noon. Right panel represents an almost entirely overcast day with a few scattered clouds around noon. Solar zenith angles are added for clarity.

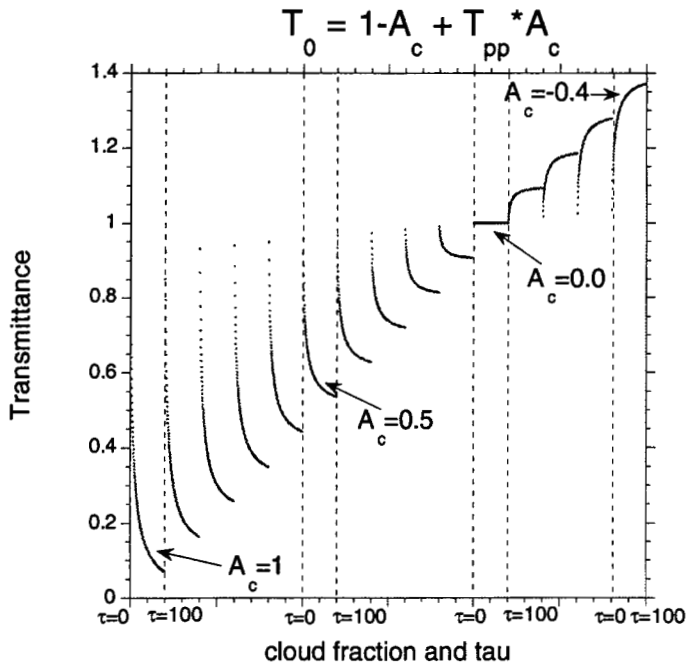

Figure 4. Transmittance T_0 as a function of optical depth τ and cloud fraction A_c. Horizontal axis consists of 15 ranges of τ from 0 to 100. Each τ-range corresponds to different A_c from $A_c = 1$ to $A_c = -0.4$ including the case of $A_c = 0$ which corresponds to $T_0 = 1$.

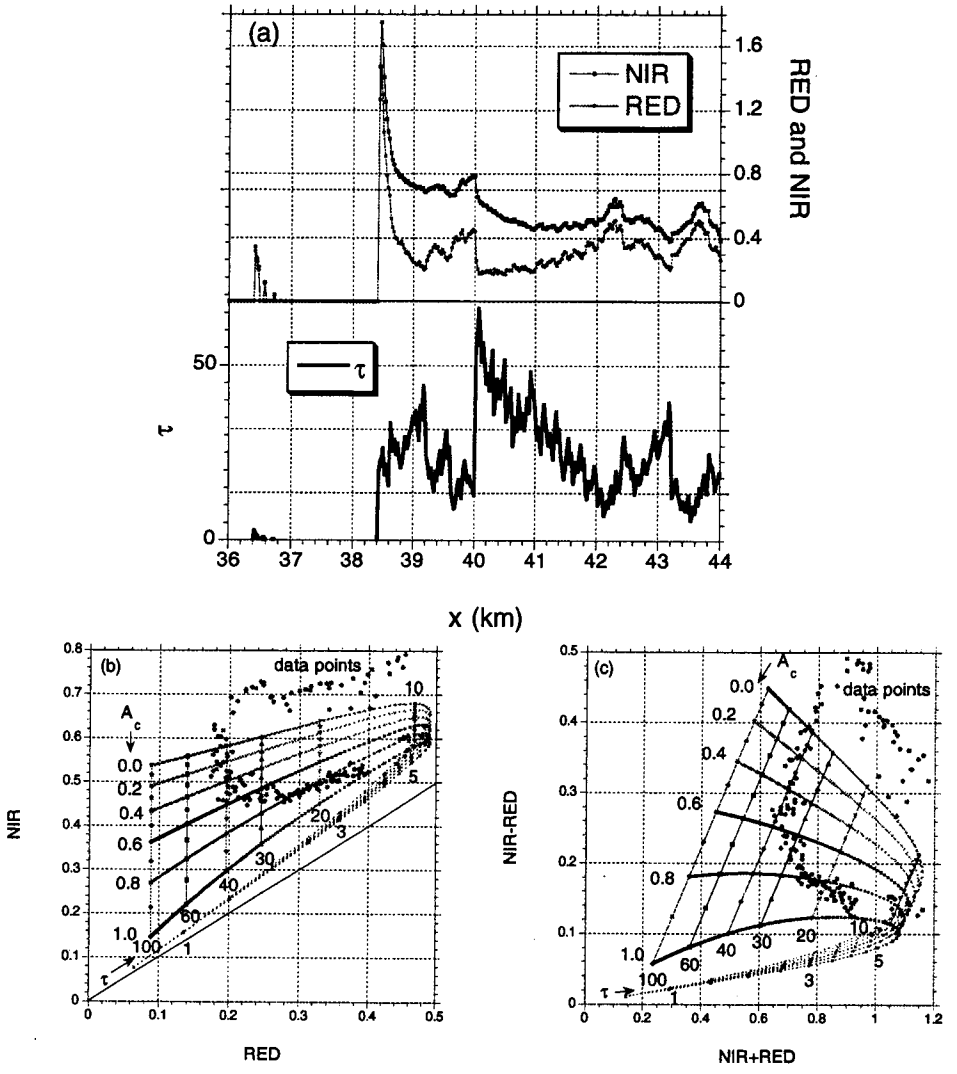

Figure 5. Zenith radiances I_{RED} and I_{NIR} for the same model as in Fig. 2. (a) An 8-km fragment of I_{RED}, I_{NIR} (top panel, right vertical axis), and optical depth τ (bottom panel, left vertical axis) versa horizontal position x (km). (b) Zenith radiances for RED and NIR as functions of optical depth τ and cloud fraction A_c [Eqs. (7a) and (7b)] calculated using DISORT (Stamnes et al., 1988); τ changes from 0.5 to 100 while A_c changes from 0.0 to 1.0. Note that both I_{RED} and I_{NIR} are double-valued functions with respect to τ. Dots correspond to data-points from panel (a) between 38.8 ($I_{NIR} < 0.8$) and 44 km (208 dots). (c) The same as in panel (b) but for $I_{NIR} - I_{RED}$ versa $I_{NIR} + I_{RED}$.

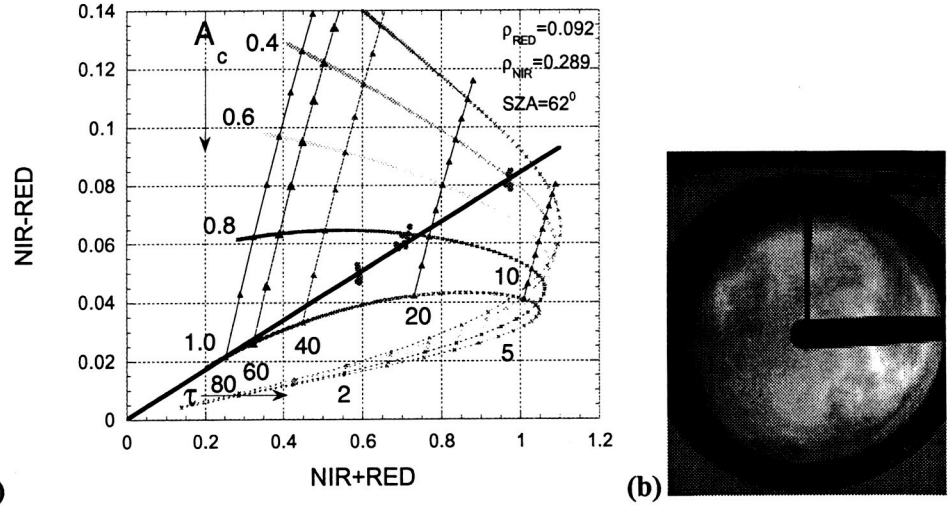

Figure 6. NIR-RED versa NIR+RED plane with Cimel radiances measured at the ARM Oklahoma site on July 28, 2002. (a) SZA = $62^0 \pm 3^0$ and surface albedos ρ_{RED}=0.092 and ρ_{NIR}=0.289. I_{RED} and I_{NIR} are calculated using DISORT. Optical depth τ changes from 0.5 to 80 while cloud fraction A_c changes from 0.2 to 1.0. 30 dots (10 for each cluster) correspond to Cimel measurements taken around 13:45, 13:58, and 14:11 UMT, respectively (towards decreasing NIR+RED). A straight line through (0,0) is the NDCI ≈ 0.08. (b) a Total Sky Image taken at 14:00 UMT with SZA=62.75^0.

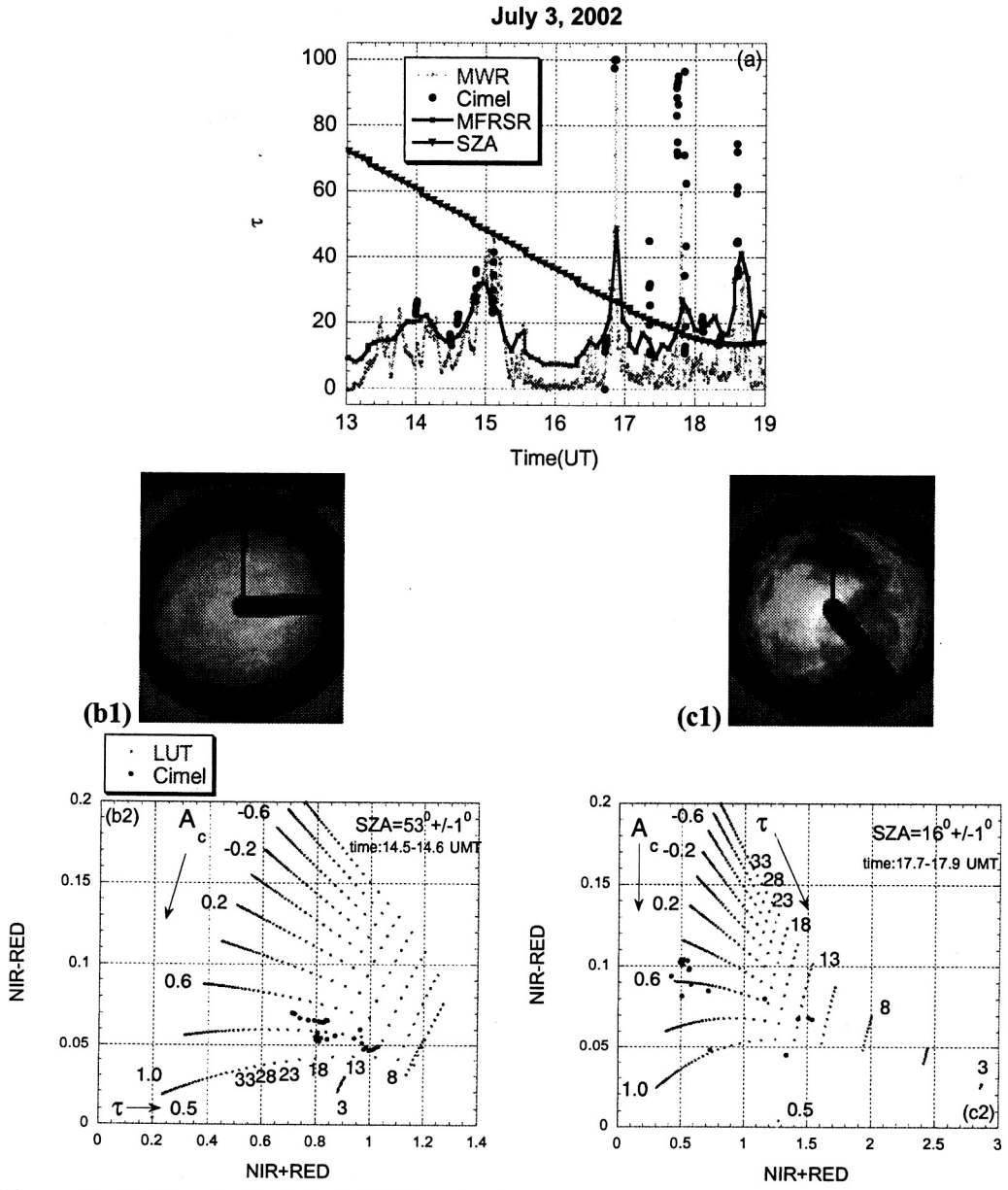

Figure 7. Retrievals for July 3, 2002 at the ARM Oklahoma site. (a) retrievals based on MWR (assuming droplet effective radius of 10 μm), Cimel radiances (using reflectances from a vegetated surface with albedos ρ_{RED}=0.119 and ρ_{NIR}=0.302), and MFRSR fluxes (using algorithm proposed in Min and Harrison, 1996). Solar zenith angle is added for convenience. (b1) a Total Sky Image for SZA = 52.3^0 taken at 14:36 UMT. (b2) LUT for SZA = 53^0 ±1^0. Optical depth τ changes from 0.5 to 100 with increment of 2.5 while cloud fraction A_c changes from -0.6 to 1.0 with increment of 0.2. 20 dots correspond to Cimel measurements taken between 14:30-14:37 UMT. (c1) the same as in (b1) but for SZA = 16.3^0 taken at 17:50 UMT. (c2) the same as in (b2) but for SZA = 16^0 ±1^0. 20 Cimel measurements were taken between 17:43-17:52 UMT.

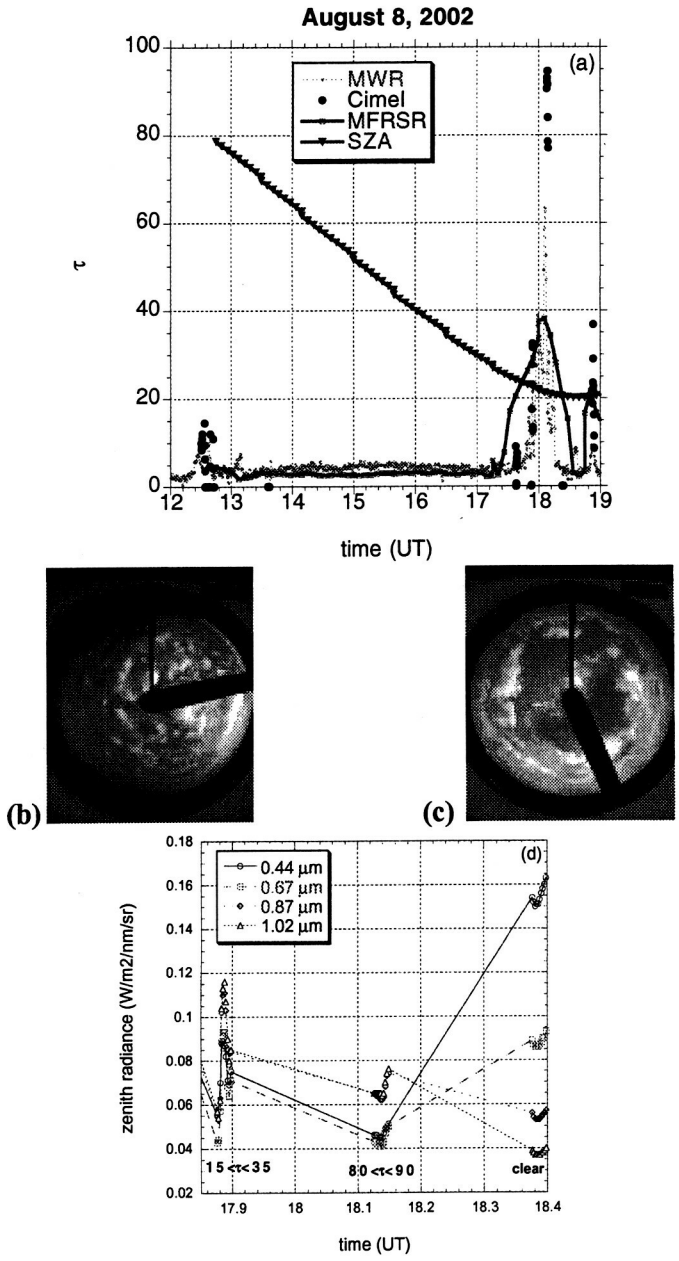

Figure 8. Retrievals for August 8, 2002 at the ARM Oklahoma site. (a) retrievals based on MWR (assuming droplet effective radius of 10 μm), Cimel radiances (surface albedos are ρ_{RED}=0.096 and ρ_{NIR}=0.338), and MFRSR (Min and Harrison, 1996). Solar zenith angle is added for convenience. (b) a Total Sky Image for SZA = 79.6^0 taken at 12:40 UMT. (c) the same as in (b) but for SZA = 21.9^0 taken at 18:00 UMT. (d) 30 min. of normalized Cimel zenith radiances at four channels: 0.44, 0.67, 0.87 and 1.02 μm.

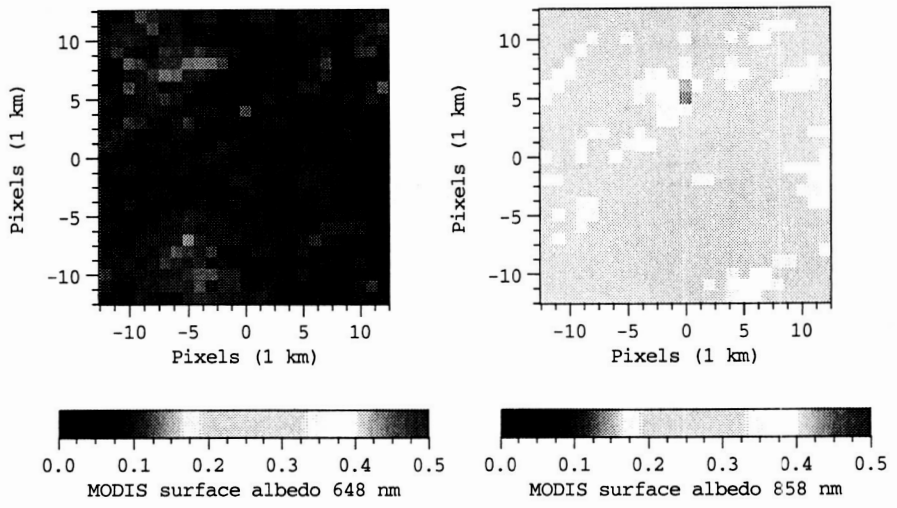

Figure 9. Surface albedo retrieved from MODIS on July 28, 2002. 25 by 25 km^2 area around the ARM site in Oklahoma; its location is at (0,0). (a) 0.648 μm, at the ARM site $\rho_{0.648} = 0.092$, averaged over (25 km)^2 $\langle\rho_{0.648}\rangle = 0.091$ with standard deviation (sdev) = 0.016. (b) 0.848 μm; at the ARM site $\rho_{0.858} = 0.289$, averaged over (25 km)^2 $\langle\rho_{0.858}\rangle$ = 0.292 with sdev = 0.043.

(for MISR on July 24, 2002: $\rho_{0.672} = 0.123$, averaged over (27.5 km)^2 $\langle\rho_{0.672}\rangle = 0.103$ with sdev = 0.017. (b) 0.867 μm; at the ARM site $\rho_{0.867} = 0.278$, averaged over (27.5 km)^2 $\langle\rho_{0.867}\rangle = 0.276$ with sdev = 0.030)

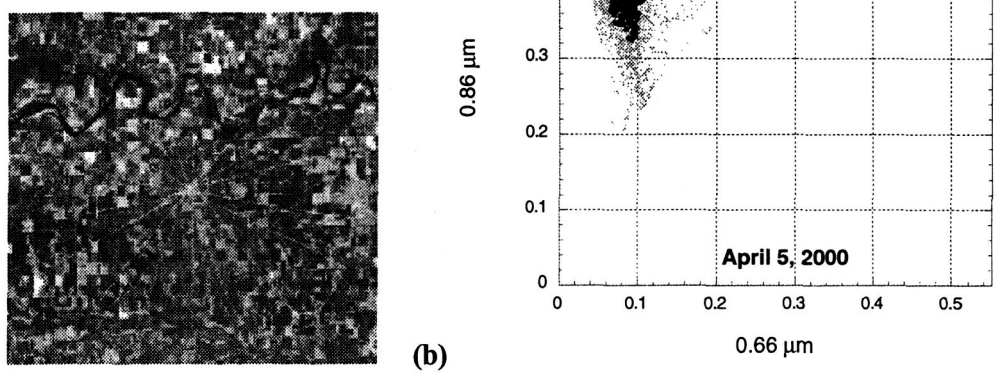

(a) (b)

Figure 10. Surface around the ARM site in Oklahoma. (a) Area around the ARM site with a daisy pattern flown by the Twin Otter aircraft on April 5, 2000 (courtesy of Alexander Trishchenko). (b) Surface albedo at 0.86 μm versa 0.66 μm measured from the aircraft by SSFR on April 5, 2000 (for details see Michalsky et al., 2003). Small gray dots correspond to all data collected around the area shown in panel (a) (roughly 10-15 km from the ARM site). Big black dots are the closest to the ARM site measurements (several middle points) taken within 0.0001 radian from the site (around 600 m). For them, $\langle\rho_{0.66}\rangle = 0.085$, sdev = 0.013 and $\langle\rho_{0.86}\rangle = 0.375$, sdev = 0.021.

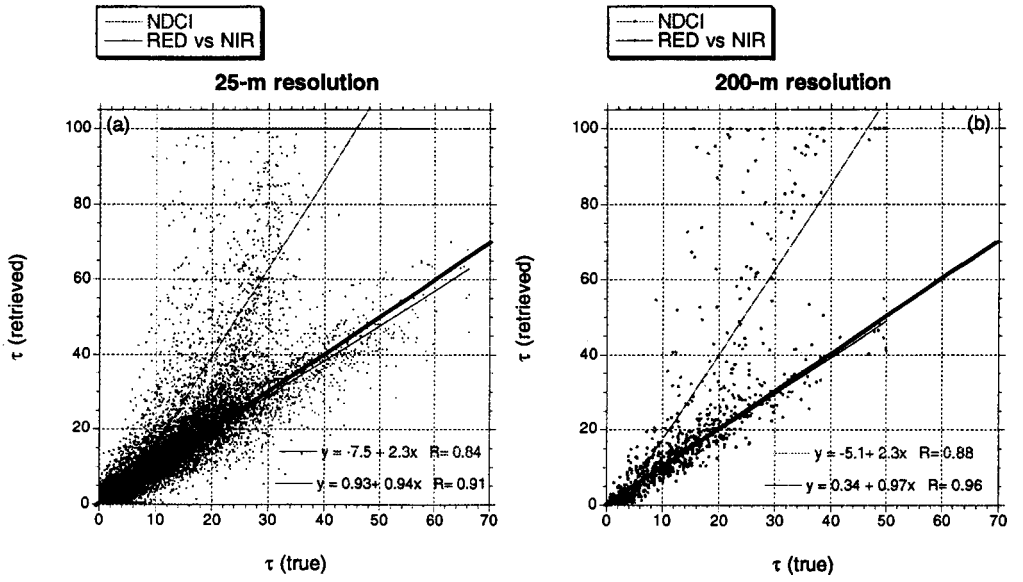

Figure 11. Scatter plot of retrieved versa true cloud optical depth for the same bounded cascade model as in Fig. 2 (Cahalan et al., 1994, Marshak et al., 1998). Cloud fraction is 81%. Ten realizations of bounded cascades are used. SZA = 60°. Two retrieval methods are compared: the "NDCI" and the "RED vs. NIR". (a) original resolution of 25 m. (b) averaged over 200 m.

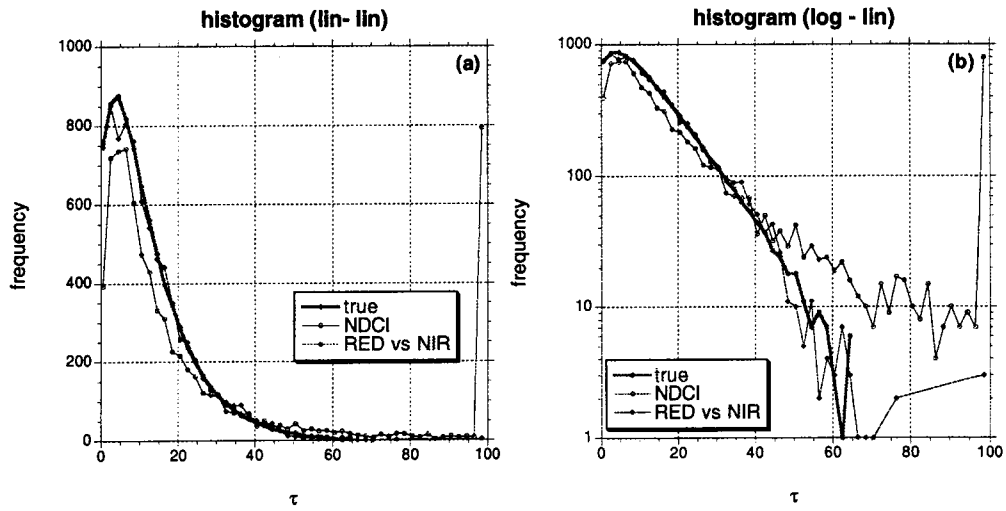

Figure 12. Histogram of cloud optical depth τ from Fig. 12a. Pixel resolution is 25 m. (a) lin-lin plot. (b) log-lin plot. (c)

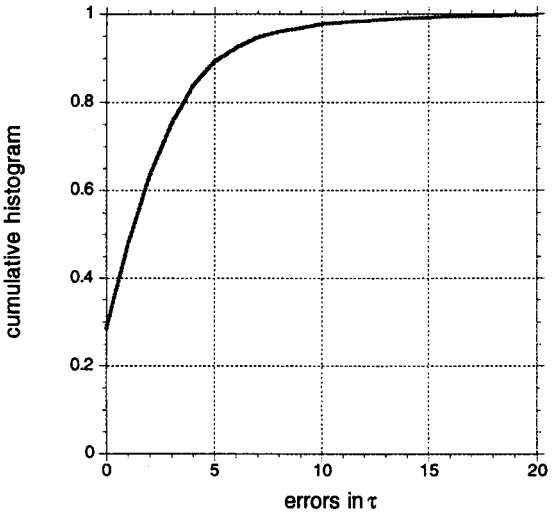

Figure 13. Cumulative histogram of absolute errors in the retrieval of cloud optical depth from Fig. 11a. Pixel resolution is 25 m.